Cell, Volume *135*

Mre11 Dimers Coordinate DNA End Bridging and Nuclease Processing in Double-Strand-Break Repair

R. Scott Williams, Gabriel Moncalian, Jessica S. Williams, Yoshiki Yamada, Oliver Limbo, David S. Shin, Lynda M. Groocock, Dana Cahill, Chiharu Hitomi, Grant Guenther, Davide Moiani, James P. Carney, Paul Russell, and John A. Tainer

SUPPLEMENTAL EXPERIMENTAL PROCEDURES

X-ray Diffraction Data Collection, Structure Determination and Refinement

Diffraction data to 2.7 Å was obtained at the Advanced Light Source beamline 5.0.2 and processed using the HKL suite (Otwinowski and Minor, 1997). Molecular replacement solutions in AmoRe (Navaza, 2001) were obtained with the structure of one protomer from the Mre11 product complex structure (Hopfner et al., 2001) as a search model (RCSB PDB code1II7). The protein portion of the structure was subjected to rigid body refinement using CNS (Brünger et al., 1998). Subsequent 2Fo-Fc and Fo-Fc electron density maps allowed for the placement of all nucleotides except for the 4T hairpin and the 3' terminal cytosine base, which appeared disordered in the crystals. The model was subjected to iterative cycles of model building with XFIT (McRee, 1999), positional, and group B-factor refinement in CNS. Final stages of refinement were conducted in REFMAC with TLS group anisotropic B-factor modeling (Murshudov et al., 1997; Winn et al., 2001) and modeling in O (v10.0) (Jones et al., 1991). In contrast to the protein density that is generally well defined, the DNA in the synaptic complex appears significantly more disordered in the crystals, likely due to Mre11 dependant disruption of base-pairing interactions.

For the Branched DNA complex, diffraction data to 2.2 Å was obtained at the Advanced Light Source beamline 12.3.1 and processed using the HKL suite (Otwinowski and Minor, 1997). Molecular replacement solutions were obtained using MOLREP (Vagin and Teplyakov, 2000) and 1II7 as the search model. Unambiguous sigma-A weighted 2Fo-Fc and Fo-Fc electron density maps calculated following rigid body fitting in REFMAC allowed placement of all nucleotides except the first three ssDNA 5' nucleotides of the DNA substrate. Positional and individual B-factor refinement using REFMAC, interspersed with iterative manual model building in O (v10.0) produced a model refined to 2.2 Å (Table S1).

ssDNA DNA docking

DOT docking was performed essentially as described in Hopfner et al. 2001. A short 3-mer ssDNA (5'-ACG-3') was docked onto the Mn^{2+} bound Mre11 dimer from the branched DNA complex.

Electrophoretic Mobility Shift Assays

Varying Mre11 protein concentrations indicated in Figures 3F and S5 were incubated with T4 PNK 5' P^{32}-labeled 40-mer ssDNA substrate (m1: 5'-CTACACTAGAAGGACAGTATTTGGTATCTGCGCTCTTGAG-3') or 40 mer dsDNA (m1 annealed to m2: 5'-CTCAAGAGCGCAGATACCAAATACTGTCCTTCTAGTGTAG-3') for 15 minutes, and complexes were separated on 6% polyacrylamide gels in 0.5 X TBE. Complexes and free DNA were detected using a phosphoimager and processed with Bio-Rad Image one software.

SAXS data processing and analysis

Guinier analysis implemented in PRIMUS (Kovnarev, 2003) was used for determination of particle radius of gyration (R_g), and GNOM (Svergun, 1992) was used to evaluate the distance distribution, P(r), functions. The maximum dimension of particles (D_{max}) were calculated with indirect Fourier transform in GNOM. Theoretical scattering was generated with CRYSOL (Svergun, 1995). Averaged *ab initio* solution structure envelopes were calculated with DAMAVER and DAMFILT (Volkov, 2003) by averaging 10 independent dummy residue models from reciprocal space minimization in GASBOR (Putnam et al., 2007; Svergun et al., 2001). Two-fold symmetry was imposed during GASBOR solution structure reconstructions of WT-Mre11. SAXS envelopes were aligned to the dimeric Mre11 structural model using SUPCOMB. Monomer-dimer content for Mre11-WT and Mre11-L61K and Mre11-L97D mutants was evaluated using OLIGOMER (Kovnarev, 2003) using GNOM smoothed data with model monomeric and dimeric Mre11 form factors generated by CRYSOL.

Endonuclease assays

ssDNA endonucleolytic cleavage of circular ϕX174 DNA was assayed at 50 ˚C. 10 μL reactions contained 250 nM of purified PfMre11 catalytic domain (1-342) variants and 1 ug of circular ϕX174 DNA in 25 mM HEPES pH 7.0, 25 mM NaCl, 5 mM $MnCl_2$. At the indicated time points, reactions were stopped by addition of EDTA to 10 mM and 2uL of 6X loading buffer containing 40% sucrose, 2.5 % SDS, 2.5 mg/mL Proteinase K. Reaction products were separted on 1.0 % agarose in 1X TAE and visualized with ethidium bromide staining.

Exonuclease assays

Steady state 2-aminopurine (2-AP) fluorescence 3'-5' exonuclease assays were performed on a Fluoromax-3 (Horiba/Yobin-Yvon) fluorimeter with constant wavelength excitation at 310 nM and emission monitored at 375nM. An increase in fluorescence at 375 nM is observed with exonucleolytic release of 2-AP from the duplex DNA, and is monitored over time for Mre11 variants. Reactions (400 μL) at 50 ˚C with branched or blunt substrates (Figure S6) and contained 250 nM protein, 1 μM 2-AP substrate, 50 mM Tris 7.5, 150 mM NaCl, 0.1 % Polyethylene glycol 6000, 2.5 % glycerol, and 1 mM $MnCl_2$. Blunt dsDNA substrate was formed by annealing equimolar amounts of exo5'1 (5'-GGCGTGCCTTGGGCGCGCTGCGGGCGG(2-AP)G-3') with exo3'1 (5'-CTCCGCCCGCAGCGCGCCCAAGGCACGCC-3') in 10 mM Tris 7.5. Branched end substrate was formed by annealing equimolar amounts of exo5'2 (5' -

GGCGTGCCTTGGGCGCGCTGCGGGCGG(2-AP)GAAAAA-3') with exo3'2 (5'-CCCCCCTCCGCCCGCAGCGCGCCCAAGGCACGCC-3') in 10 mM Tris 7.5.

S. pombe strain construction

Methods and growth media for *S. pombe* genetics were as previously described (Moreno et al., 1991). All strains used in this study are listed in Table S4. Site-directed mutagenesis was performed with the Stratagene QuikChange kit. The wild type and mutagenized plasmids containing *mre11* C-terminally myc-tagged and flanked by upstream and downstream sequences were digested with *Kpn*I-*Not*1, gel-purified, and used to replace $mre11^{+}$ in strain PR109. Gene replacement was confirmed by PCR and sequencing was performed to verify the presence of the correct point mutation(s).

HO ChIP Assay

HO endonuclease was expressed under thiamine-repressible *nmt1* promoter. Phospho-H2A, Mre11 and Nbs1 were immunoprecipitated from YYY4182 (*arg3::HO site ars1:HO endonuclease:ars1 mre11-H134S-13myc nbs1-5xFLAG*) using anti-phospho H2A antibody, anti-myc antibody and anti-FLAG antibody, respectively. Ctp1 was immunoprecipitated from YYY4181 (*arg3::HO site ars1:HO endonuclease:ars1 mre11-H134S-13myc nbs1-5xFLAG ctp1-TAP*) using rabbit IgG-conjugated Dynabeads (Dynal). In whole cell extract (WCE), 5 bands are equally amplified.

Figure Preparation

The molecular volumes in Figures 3D, 4A, 4F, 4G and 7A were generated with SITUS (Wriggers and Birmanns, 2001) and rendered using VMD (Humphrey et al., 1996). All other molecular diagrams were created using Pymol (http://www.pymol.org).

SUPPLEMENTAL REFERENCES

Brünger, A. T., Adams, P. D., Clore, G. M., DeLano, W. L., Gros, P., Grosse-Kunstleve, R. W., Jiang, J. S., Kuszewski, J., Nilges, M., Pannu, N. S., *et al.* (1998). Crystallography & NMR system: A new software suite for macromolecular structure determination. Acta Crystallogr D Biol Crystallogr *54 (Pt 5)*, 905-921.

Hopfner, K. P., Karcher, A., Craig, L., Woo, T. T., Carney, J. P., and Tainer, J. A. (2001). Structural biochemistry and interaction architecture of the DNA double-strand break repair Mre11 nuclease and Rad50-ATPase. Cell *105*, 473-485.

Humphrey, W., Dalke, A., and Schulten, K. (1996). VMD: visual molecular dynamics. J Mol Graph *14*, 33-38, 27-38.

Jones, T. A., Zou, J. Y., Cowan, S. W., and Kjeldgaard, M. (1991). Improved methods for building protein models in electron density maps and the location of errors in these models. Acta Crystallogr A *47 (Pt 2)*, 110-119.

Kovnarev, P. V., Volkov, A.V., Sokolova, A.V., Koch, M.H.J., and Svergun, D.I. (2003). PRIMUS: a Windows PC-based system for small-angle scattering data analysis. J Appl Cryst *36*, 1277-1282.

McRee, D. E. (1999). XtalView/Xfit--A versatile program for manipulating atomic coordinates and electron density. J Struct Biol *125*, 156-165.

Moreno, S., Klar, A., and Nurse, P. (1991). Molecular genetic analysis of fission yeast Schizosaccharomyces pombe. Methods Enzymol *194*, 795-823.

Murshudov, G. N., Vagin, A. A., and Dodson, E. J. (1997). Refinement of macromolecular structures by the maximum-likelihood method. Acta Crystallogr D Biol Crystallogr *53*, 240-255.

Navaza, J. (2001). Implementation of molecular replacement in AMoRe. Acta Crystallogr D Biol Crystallogr *57*, 1367-1372.

Otwinowski, Z., and Minor, W. (1997). Processing of X-ray Diffraction Data Collected in Oscillation Mode, In Methods in Enzymology, C. W. Carter, Jr., and R. M. Sweets, eds. (New York: Academic Press), pp. 307-326.

Svergun, D. I. (1992). Determination of the regularization parameter in indirect-transform methods using perceptual criteria. J Appl Crystallogr *25*, 495-503.

Svergun, D. I., Barberato, C., and Koch, M.H.J. (1995). Crysol—a program to evaluate X-ray solution scattering of biological macromolecules from atomic coordinates. . J Appl Crystallogr *28*, 768-773.

Svergun, D. I., Petoukhov, M. V., and Koch, M. H. (2001). Determination of domain structure of proteins from X-ray solution scattering. Biophys J *80*, 2946-2953.

Vagin, A., and Teplyakov, A. (2000). An approach to multi-copy search in molecular replacement. Acta Crystallogr D Biol Crystallogr *56*, 1622-1624.

Volkov, A. V., and Svergun, D.I. (2003). Uniqueness of ab initio shape determination in small-angle scattering. J Appl Crystallogr *36*, 860-864.

Winn, M. D., Isupov, M. N., and Murshudov, G. N. (2001). Use of TLS parameters to model anisotropic displacements in macromolecular refinement. Acta Crystallogr D Biol Crystallogr *57*, 122-133.

Wriggers, W., and Birmanns, S. (2001). Using situs for flexible and rigid-body fitting of multiresolution single-molecule data. J Struct Biol *133*, 193-202.

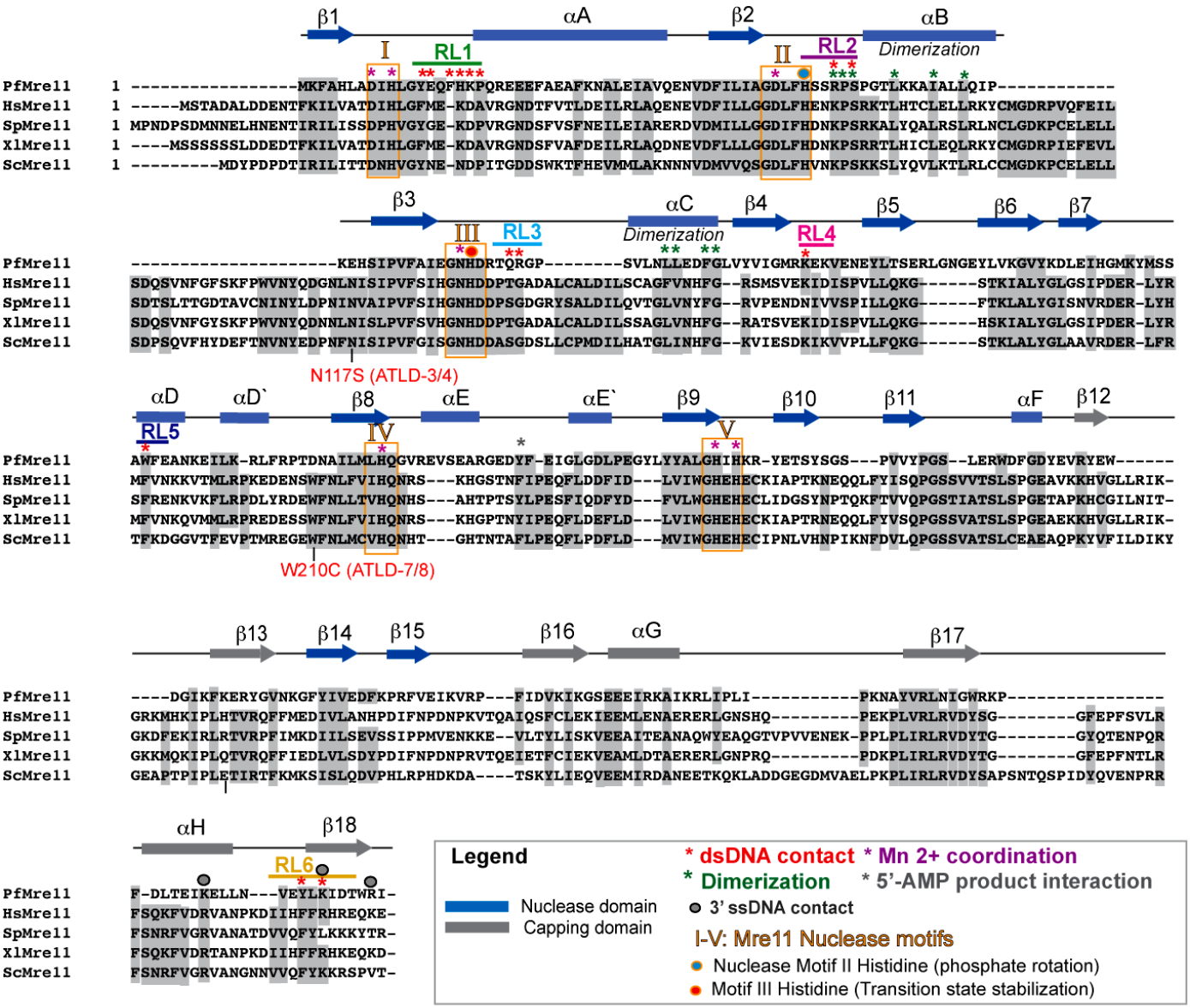

Figure S1. Structure based sequence alignment of Mre11 homologs
Secondary structures for the nuclease domain (blue), nuclease-capping domain (grey) are shown. See legend inset for residue specific functional annotations.

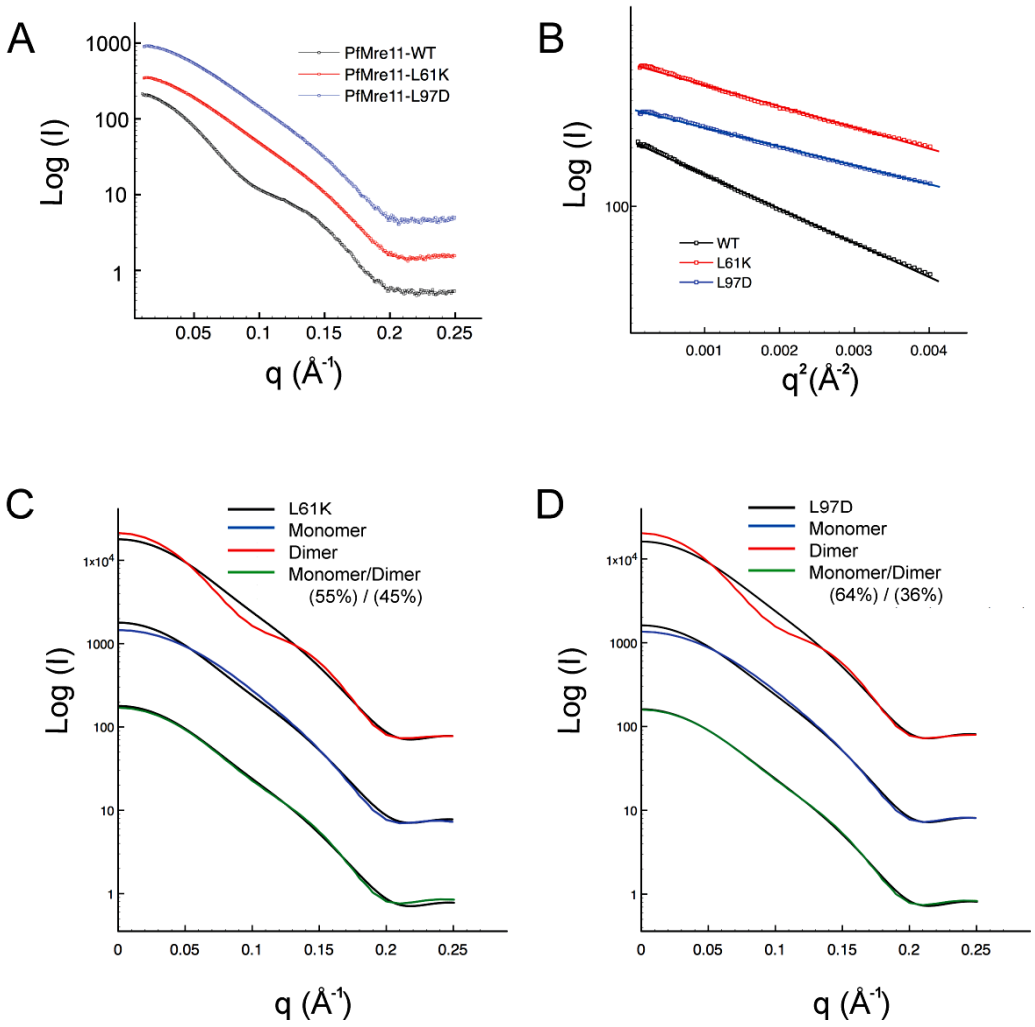

Figure S2. Small angle X-ray scattering analysis of Mre11 dimerization mutants.
(A) SAXS profiles for WT(black), L61K (red), and L97D (blue). Log of scattered intensity versus q is plotted for the range 0.010 $Å^{-1}$ - 0.250 $Å^{-1}$. The curves have been offset for visualization.
(B) Guinier plots of WT(black) , L61K (red), and L97D (blue) PfMre11 proteins.
(C,D) Small angle X-ray scattering analysis of Mre11 dimerization mutants. Monomer-dimer content for Mre11-L61K (C) and Mre11-L97D (D) was estimated using OLIGOMER.

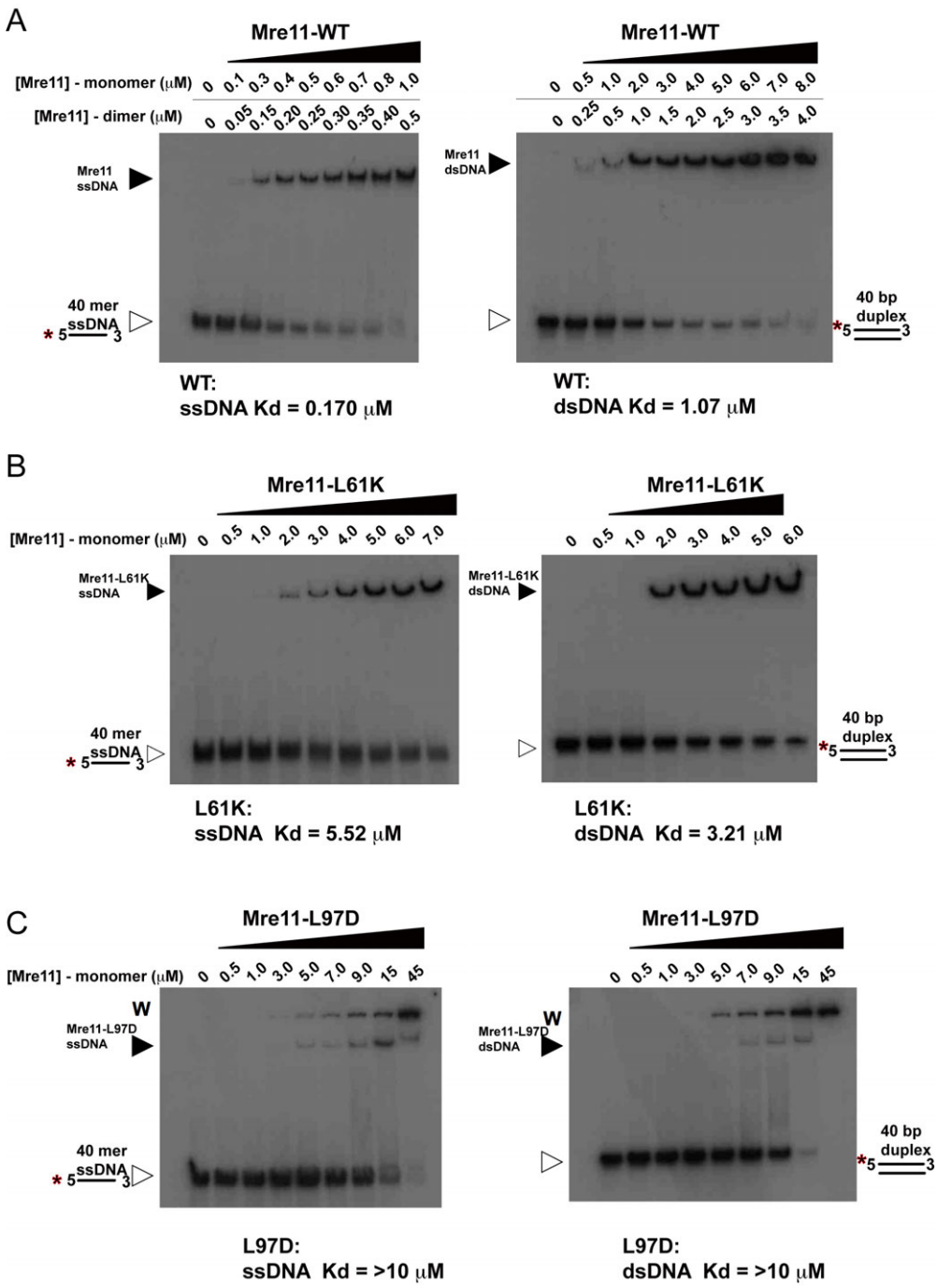

Figure S3. EMSA analysis of Mre11 dimerization variant DNA binding. Binding affinities are expressed in terms of mols of Mre11 dimer for the WT protein, and mols of Mre11 monomer for the L61K and L97D mutants.

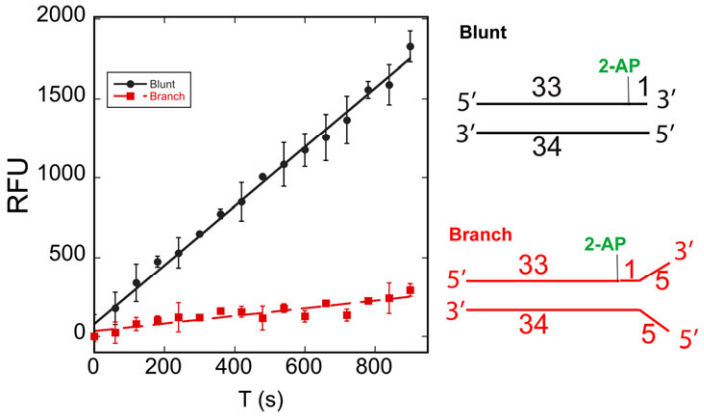

Figure S4. PfMre11 exonuclease activity on blunt and branched 2-aminopurine containing DNA substrates.

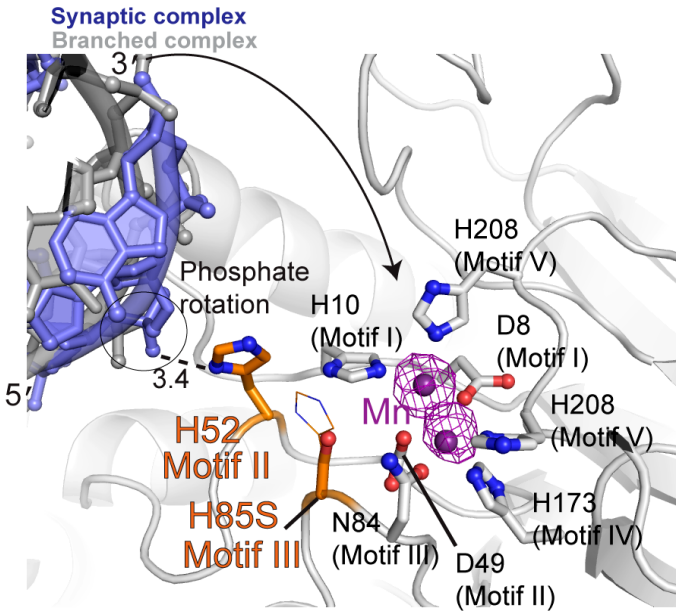

Figure S5. Metal binding is preserved in the Mre11-H85S mutant
The motif III histidine H85S mutation used for crystallization of the Mre11-branched DNA complex is exposed to solvent (H85S), and does not directly coordinate manganese. The closest side-chain:Mn^{2+} distances for H52 (7.1 Å) and H85 (3.9 Å) imidazole rings is much greater than observed for metal coordinating motif I, IV, and V histidines (2.15-2.35 Å). Mn^{2+} in the crystals was not added during crystallization and originates from trace sources in expression media in E. coli, showing that metal coordination capacity is robust for the Motif III histidine substitution H85S. σ-A weighted Fo-Fc electron density map (purple) calculated prior to building metal sites and DNA for the synaptic complex is displayed contoured at 3.0 σ. H52 from motif II is required to direct the 3' terminus into the active site for 3'-5' exonucleolysis. Mutation of H52 to serine would lose the positively charged H52 imidazole ring hypothesized to directly bridge and direct the 3' terminus into the active site during 3'-5' exonucleolysis.

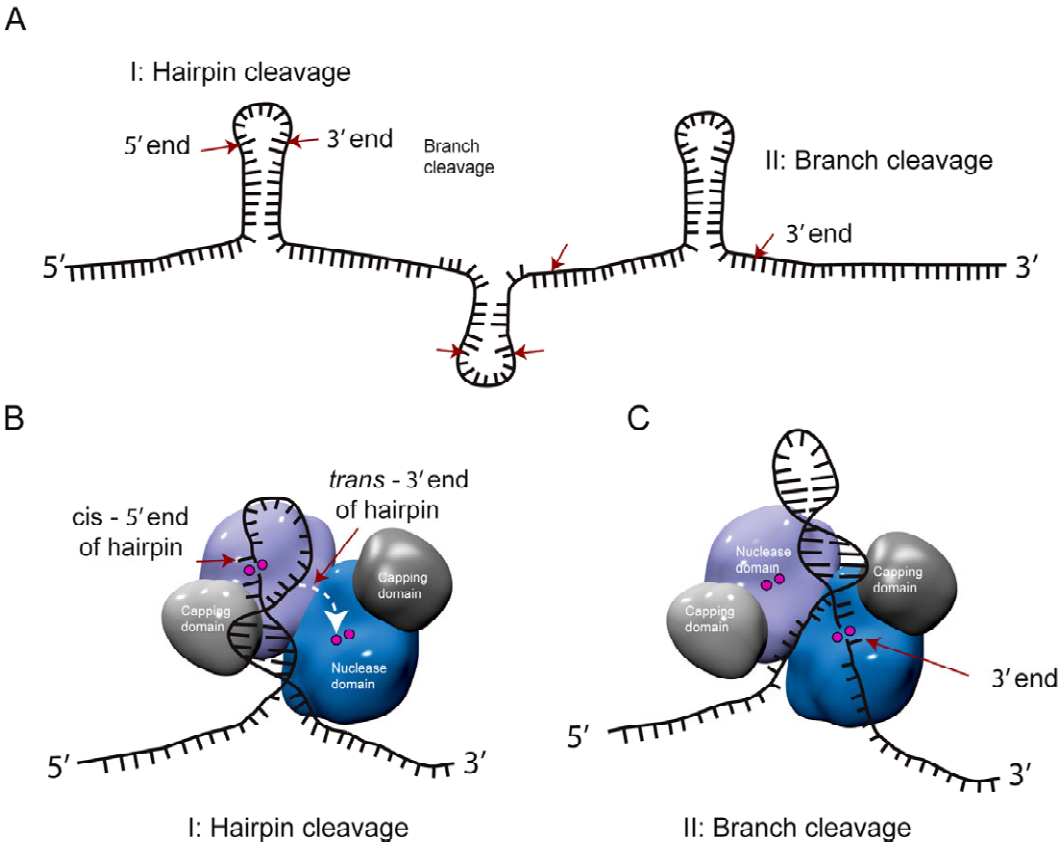

Figure S6. Mre11 structure specific endonuclease activities.
(A) Mre11 cleaves ssDNA regions on 5' and '3 ends of hairpins, and 3' ends of branch regions. These Rad50 dependant structure specific endonuclease activities may contribute to ssDNA endonucleolytic cleavge by acting on transient secondary structures formed within exposed stretches of ssDNA.
(B) Structural model for Mre11 cleavage activity on 5' and 3' ends of DNA hairpins.
(C) Structural model for Mre11 cleavage at 3' ends of branched structures.

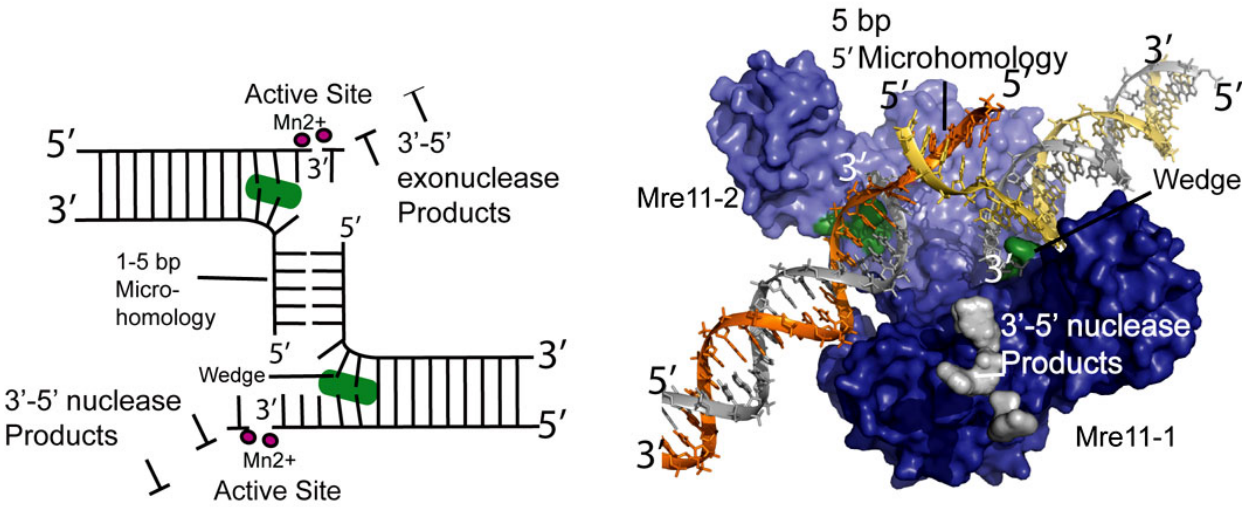

Figure S7. Structural model for Mre11 mediated 5'-microhomology repair.
The structural model (right) for the Mre11-catalysed 5' microhomology pairing reaction (left) is based on the Mre11-DNA synaptic complex. 5'-microhomology pairing activity combines Mre11 DNA end tethering, DNA unwinding, and 3'-5' exonucleolytic activities. Human Mre11 and the *S. cerevisiae* MRX complex also directly promote ligase-dependent joining of non-homologous DNA molecules *in vitro*. For hMre11, this activity proceeds through a 5'-microhomology search mechanism where Mre11 catalyzes pairing and ligation of heterologous substrates bearing short stretches of homology near their 5'-termini (Paull and Gellert, 1998). The three Mre11 activities presumably act in concert to regress the 3' strand of two substrate DNAs while simultaneously promoting duplex pairing and the search for short (3-5 bp) segments of complementary sequence in the 5' strands. Two juxtaposed 5' DNA ends pair as 3' ends are regressed by 3'-5' exonuclease activity. Disruption of base pairing, and separation of duplex strands liberates 5' termini for inter-strand duplex pairing across the dimer cleft, aiding 5' microhomology end joining reactions. The spacing of the two duplex DNAs across the cleft predicts that microhomology pairing would be limited to 1-5 DNA base pairs. This molecular metric corresponds to the length of short sequence homologies generated by human Mre11 (Paull and Gellert, 1998).

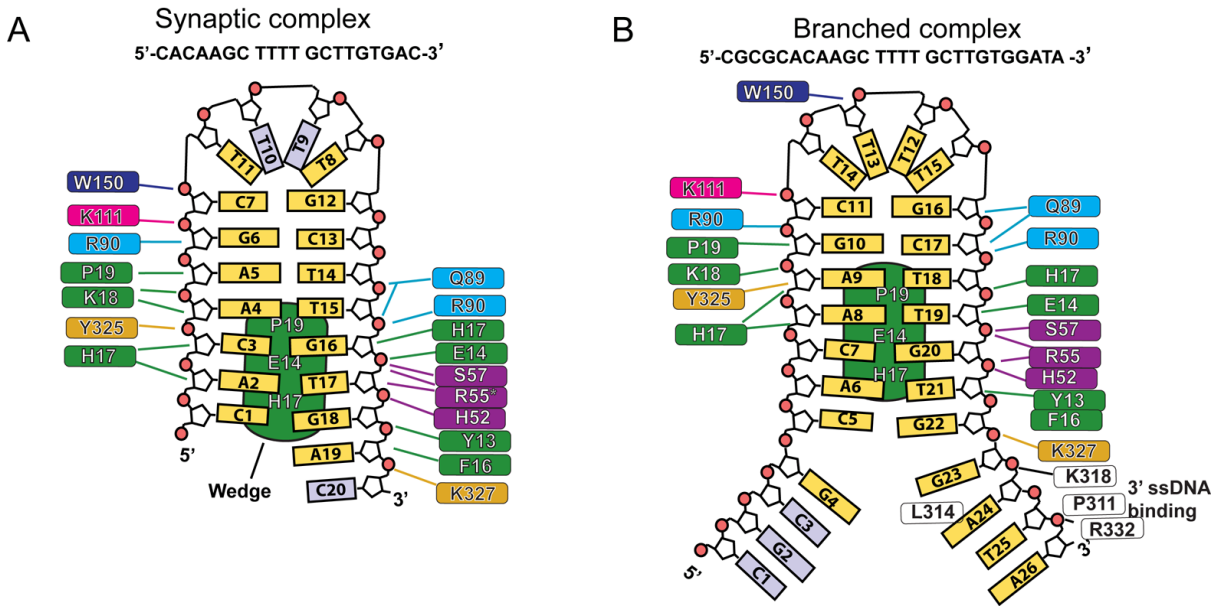

Figure S8. Schematics for DNA protein contacts in Mre11 DNA complexes
(A) DNA-protein interactions in the Mre11-synaptic DNA complex. Residue contacts are colored according to the six DNA binding regions (RL1 (green), RL2 (purple), RL3 (turquoise), RL4 (pink), RL5 (dark blue) and RL6 (yellow). Unobserved nucleotides in the crystal are shaded light blue. Observed nucleotides are yellow.
(B) DNA-protein interactions in the Mre11-branched DNA complex. Residue and nucleotide coloring is the same as that for panel "A". Additional 3' ssDNA interacting residues are white with black lettering.

Table S1: X-ray data collection phasing, and refinement statistics

Data Collection			
Complex		Synaptic DNA complex	Branched DNA complex
Beamline		ALS-BL5.0.2	ALS-BL12.3.1
Space group		C222	$P2_12_12_1$
Cell dimensions	a (Å)	98.48	77.12
	b (Å)	106.07	88.13
	c (Å)	76.67	137.41
Wavelength (Å)		0.9759	1.1159
Resolution range (Å)		20-2.70	50-2.20
Unique reflections		10769	47737
Average redundancy		4.8	6.1
Data coverage: total/final shell (%) [1]		94.5/83.0	98.5/95.4
$\langle I/\sigma I \rangle$ total/final shell [1]		17.6/3.6	20.1/3.2
R_{sym} total/final shell (%)[2]		8.5/36.5	7.1/52.1
Refinement Statistics			
Resolution range(Å)		20-2.7	50-2.2
R_{work} [3]/R_{free} (%)[4]		22.8/27.8	20.0/24.6
Refined atoms	Protein	2754	5500
	DNA	348	473
	Solvent	83	308
	Mn	0	4
R.m.s. deviations	Bonds (Å)	0.005	0.011
	Angles (°)	0.983	1.39
Mean B-factors (Å^2)		42.4[5]	43.3
Ramachandran	Core	90.4	89.9
	Allowed	8.9	9.3
	Generous	0.0	0.3
	Disallowed	0.7	0.5

[1] Final shell: 2.80 – 2.70 Å (Synaptic complex); 2.28 – 2.20 Å (Branched complex)
[2] $R_{merge}=\Sigma |(I_{hkl}) - \langle I \rangle| / \Sigma(I_{hkl})$ where I_{hkl} is the integrated intensity of a given reflection.
[3] $R_{work} = \Sigma_h|F_o(h) – F_c(h)| / \Sigma_h | F_o(h)|$, where $F_o(h)$ and $F_c(h)$ are observed and calculated structure factors. [4] R_{free} calculated with 5% of all reflections excluded from refinement stages. No $I/\sigma I$ cutoff was used in the refinement.
[5] B-factors for the synaptic complex are from individual B-factor refinement following TLS group anisotropic B-factor modeling in REFMAC.

Table S2. Structural Parameters of Mre11 Dimerization from Analytical Gel Filtration

Sample [a] or Model	Apparent MW (Superdex200) (kDa)	Oligomeric State
Mre11 WT	73.8	Dimer
Mre11 L61K	36.4	Monomer
Mre11 L97D	36.7	Monomer
Mre11 Dimer structural model [b]	81.6 (theoretical MW)	
Mre11 monomer structure model [b]	40.8 (theoretical MW)	

[a]Samples at ~0.5 mg/mL (~12.5 μM) final concentration

Table S3. Structural Parameters of Mre11 Dimerization from SAXS

Sample [a] or Model	R_g (Å)	χ^2 (Monomer) [b]	χ^2 (Dimer) [b]	χ^2 (Monomer/ Dimer) [b]	Oligomeric State [a]
Mre11 WT	34.6	9.8	3.1	n/a	Dimer
Mre11 L61K	27.1	3.3	4.9	2.0	Monomer (55%) Dimer (45%)
Mre11 L97D	25.9	2.5	5.3	1.0	Monomer (64%) Dimer (36%)
Mre11 Dimer structural model [b]	33.1				
Mre11 monomer structure model [b]	25.0				

[a] Samples at 10 mg/mL (250 μM)
[b] χ^2 Fitting statistics from CRYSOL and OLIGOMER. Fitting is not improved with monomer-dimer modeling for WT-Mre11.

Table S4. *S. pombe* strains used in this study

Strain	Genotype	Source or reference
PR109 (*Untagged Mre11WT*)	*h⁻ leu1-32 ura4-D18*	Lab stock
YYY4165	*h⁻ leu1-32 mre11::kanMX6*	This study
JW4166 (*Mre11+*)	*h⁺ leu1-32 ura4-D18 mre11-13myc:kanMX6*	This study
JW4167	*h⁺ leu1-32 ura4-D18 mre11-L77K-13myc:kanMX6*	This study
JW4168	*h⁺ leu1-32 ura4-D18 mre11-L154D-13myc:kanMX6*	This study
JW4169	*h⁺ leu1-32 ura4-D18 mre11-L77K L154D-13myc:kanMX6*	This study
JW4170	*h⁻ leu1-32 ura4-D18 mre11-H68S-13myc:kanMX6*	This study
JW4171	*h⁻ leu1-32 ura4-D18 mre11-H134S-13myc:kanMX6*	This study
OL4172	*h⁻ leu1-32 ura4-D18 mre11-H134S-13myc:kanMX6 pku80::hph*	This study
OL4173	*h⁺ leu1-32 ura4-D18 mre11-H134S-13myc:kanMX6 pku80::hph exo1::ura4⁺*	This study
OL4174	*h⁺ leu1-32 ura4-D18 mre11-H134S-13myc:kanMX6 exo1::ura4⁺*	This study
OL4175	*h⁻ leu1-32 ura4-D18 exo1::ura4⁺*	This study
OL4176	*h⁻ leu1-32 ura4-D18 pku80::hph exo1::ura4⁺*	This study
SC4083	*h⁻ leu1-32 ura4-D18 pku80::hph*	Cavero et al., 2006
OL4177	*h⁻ leu1-32 ura4-D18 mre11::kanMX6*	This study
OL4178	*h⁻ leu1-32 ura4-D18 mre11::kanMX6 pku80::hph*	This study
OL4179	*h⁻ leu1-32 ura4-D18 mre11::kanMX6 pku80::hph exo1::ura4⁺*	This study
OL4180	*h⁻ leu1-32 ura4-D18 mre11::kanMX6 exo1::ura4⁺*	This study
YYY4181	*h⁰ leu1-32 ura4-D18 his3-D1 arg3::HO site(kanMX6) ars1:nmt-(HO endonuclease):ampR:his3⁺:ars1 mre11-H134S-13myc:kanMX6 nbs1-5flag:kanMX6 ctp1-TAP:hph*	This study
YYY4182	*h⁰ leu1-32 ura4-D18 his3-D1 arg3::HO site(kanMX6) ars1:nmt-(HO endonuclease):ampR:his3⁺:ars1 mre11-H134S-13myc:kanMX6 nbs1-5flag:kanMX6*	This study